

LA-UR-11-4996

*Approved for public release;
distribution is unlimited.*

Title: Simulating the Dynamics of Wind Turbine Blades:
Part I, Model Development and Verification

(Manuscript)

Author(s): Mark G. Mollineaux, Stanford University
Kendra L. Van Buren, Clemson University
François M. Hemez, Los Alamos National Laboratory
Sezer Atamturktur, Clemson University

Intended for: Wind Energy, August 2011



Los Alamos National Laboratory, an affirmative action/equal opportunity employer, is operated by the Los Alamos National Security, LLC for the National Nuclear Security Administration of the U.S. Department of Energy under contract DE-AC52-06NA25396. By acceptance of this article, the publisher recognizes that the U.S. Government retains a nonexclusive, royalty-free license to publish or reproduce the published form of this contribution, or to allow others to do so, for U.S. Government purposes. Los Alamos National Laboratory requests that the publisher identify this article as work performed under the auspices of the U.S. Department of Energy. Los Alamos National Laboratory strongly supports academic freedom and a researcher's right to publish; as an institution, however, the Laboratory does not endorse the viewpoint of a publication or guarantee its technical correctness.

RESEARCH ARTICLE

Simulating the dynamics of wind turbine blades: part I, model development and verification

Mark G. Mollineaux¹, Kendra L. Van Buren², François M. Hemez³ and Sezer Atamturktur²

¹ Department of Civil and Environmental Engineering, Stanford University, 473 Via Ortega, Room 314, Mail Code 4020, Stanford, California 94305, USA

² Department of Civil Engineering, Clemson University, Lowry Hall, Box 340911, Clemson, South Carolina, 29634-0911, USA

³ Los Alamos National Laboratory, XTD-Division (XTD-3), Mail Stop T087, Los Alamos, NM 87545, USA

ABSTRACT

In the state of the art of modeling and simulation of wind turbines, verification and validation (V&V) is a somewhat under-developed field. The purpose of this paper is to spotlight the process of a completely integrated V&V procedure, as it is applied to a wind turbine blade. The novelty, besides illustrating the application of V&V to blade modeling, is to challenge the conventional separation between verification and validation activities. First, simple closed-form solutions for bending stress, torsional stress and mode shapes of a hollow cylinder are derived analytically to verify the ANSYS finite element software. Shell-281 elements are used to approximate these closed-form solutions and demonstrate that the software runs properly. The grid convergence index is used to quantify the degree of numerical uncertainty that results. Next, model development and verification activities are applied to the CX-100 blade designed at the Sandia National Laboratories. A three-dimensional model is developed based on the actual geometry of the CX-100 blade. For simplicity, the model assumes smeared cross sections with uniform, isotropic material properties. Solution verification is performed to quantify the numerical uncertainty due to mesh discretization of the finite element model. The mesh refinement study provides evidence that the model leads to numerical solutions located in the regime of asymptotic convergence. We depart from the conventional V&V paradigm by proposing that the level of mesh discretization should be based on an assessment of experimental variability. Instead of choosing the mesh size 'in a vacuum', it is selected such that the overall numerical uncertainty caused by truncation effects is similar to, or smaller than, the test-to-test variability. This rationale guarantees that predictions are sufficiently accurate relative to the level of uncertainty with which physical tests can be replicated. Part II of this work highlights the V&V steps implemented to quantify sensitivities of the model and further quantify the prediction uncertainty caused by our imperfect knowledge of the idealized material description. Copyright © 2012 John Wiley & Sons, Ltd.

KEYWORDS

wind turbine blades; verification and validation; solution uncertainty; numerical uncertainty

Correspondence

Kendra L. Van Buren, Department of Civil Engineering, Clemson University, Lowry Hall, Box 340911, Clemson, South Carolina 29634-0911, USA.

E-mail: klvan@clemson.edu

Received 8 September 2011; Revised 6 March 2012; Accepted 15 April 2012

1. INTRODUCTION

Wind power in the USA has the potential to supply a major amount of electricity. This objective is outlined by the '20% by 2030' initiative of the U.S. Department of Energy (DOE), whereby DOE identifies wind energy as a viable source to contribute to 20% of installed energy, assuming a 39% increase in demand for electricity.¹ This ambitious objective has enormous implications for the wind power market that supplied only 2% of electrical energy in the USA by the end of 2009.

For the increased use of wind energy to be realized, the cost of energy needs to decrease significantly. This can be facilitated by understanding wind turbine failures so that they can be better prevented. It has been shown that damage to wind turbine components, such as the generator, drive train, hub, gearbox and blades, can result in periods of downtime,

in which the wind turbine is temporarily taken out of service.² The combination of repair and loss in energy production during downtime can negatively impact the sales and profitability model of an entire wind plant.³ This study focuses on wind turbine blades because they are first in line to capture the kinetic energy of the wind and also produce all of the loads for the entire system.⁴ Furthermore, even minor damage to blades can progress to serious secondary damage to the entire wind turbine system.⁵

Modeling and simulation (M&S) will play an indispensable role in the development of future wind turbine blades, whether it is to understand blade vibrations, simulate the loading environment that vibrations generate on the main shaft assembly or predict the occurrence and severity of structural damage. It is also forecasted that M&S will be essential to filter a wide variety of plausible design concepts down to the most effective ones.⁶

The current state of the practice of M&S and availability of computing resources for engineering applications necessitate a certain trade-off between the implementation of large-scale, high-fidelity models and the use of simplified models that are much less computationally expensive. It is desirable to assess, for example, the potential consequences of structural damage on blade performance, but large-scale models are too demanding of computational resources to be implemented for rapid prototyping and diagnostics. For this reason, the study presented in this paper and companion publication⁷ proposes **to develop a finite element model that, although simplified as much as possible, still captures the main dynamics of interest**. Importantly, this trade-off is quantified, allowing the process to run along methodical, and not arbitrary, grounds. V&V activities discussed in these two manuscripts are essential steps of the model development process to guarantee that the simplifications introduced are justified for the intended purpose.

In this study, V&V activities are applied in the development of a finite element (FE) model of the CX-100 wind turbine blade using NuMAD,⁸ pre-processing software developed at the Sandia National Laboratories (SNL) and imported to ANSYS version 12.1. The CX-100 wind turbine blade is a 9 m research blade developed at the SNL in 2002 as a part of ongoing research efforts to improve the performance of wind turbine blades.⁶ The CX-100 was developed for the purpose of studying the performance, and reducing the energy production costs, of wind turbine blade designs that utilize lightweight carbon fiber material to reinforce the spar cap.⁹ Our main goals are to develop a validated simulation of the low-frequency dynamics and quantify the uncertainty that arises, both from the potential lack of resolution in calculations and from uncertainty relating to parameter estimation. The dynamics of interest for this study are the first three flap-wise bending modes. The model developed herein relies on a strong simplification: the cross-sectional areas of the blade are smeared, using isotropic material properties, instead of modeling the multiple composite layers embedded in an epoxy matrix. Credibility of the simulation rests on our ability to quantify various sources of numerical, modeling and experimental uncertainties.

The manuscript is organized as follows. Section 2 briefly discusses pertinent literature from the discipline of wind turbine blade modeling and testing. An upper bound of solution uncertainty is derived in Section 3 to guide the selection of an appropriate level of mesh discretization. Code verification activities are presented in Section 4. Section 5 discusses the experimental setup and measurements collected from vibration testing. Finally, the upper bound of solution uncertainty (derived in Section 3) is combined to the experimental variability (estimated in Section 5) to arrive at a rational and scientifically defensible selection of mesh resolution in Section 6.

2. REVIEW OF PERTINENT LITERATURE

An issue relating to the development of FE models was revealed in 2005, when a code verification study of shell elements was performed to explore whether the implementation of shell elements in FEA software (which have since been modified) was appropriate to model the torsional response of wind turbine blades.¹⁰ The study found that shell elements modeled with nodes at the exterior surface for a hollow cylinder deviated significantly from the closed-form solution for torsional stress. This error was especially unfortunate in that the results for the shell elements diverged from the exact solution as the mesh was refined. This formulation, in which the nodes of the shell element are at the exterior surface (as opposed to the middle), is common in wind turbine blade modeling. This deficiency of earlier shell elements shows that a simple code verification study is necessary to establish credibility of numerical simulations because it brings into question the dependability of FE predictions and M&S efforts performed prior to this finding.

Additionally, verification campaigns frequently execute mesh refinement by less than rigorous methods, in which a mesh is ultimately selected at an arbitrary density. A common practice is to select the resolution of a mesh discretization by completely qualitative methods or simply to obey the constraints defined by the computational resource available. To effect truly credible predictions, verification activities should include quantitative methods of determining the uncertainty of numerical simulations.¹¹ Selecting a proper mesh discretization can be achieved by several helpful metrics for extrapolation and quantification of truncation error, which are well understood.¹²

Experimental modal analysis (EMA) has been used to study the vibration response of wind turbine blades. There are two typical testing configurations in EMA: free-free, in which the testing specimen is suspended in the air (using straps or cushions) such that the response is as though there is no imposed boundary condition, and fixed free, in which movement is constrained at the support of the testing specimen. Previous studies discuss that the use of a free-free boundary condition,

although less applicable to reality, is common because it is easy to implement under laboratory conditions.^{13,14} In comparison, it is significantly more difficult to achieve an idealized fixed-end condition in experimental testing of wind turbine blades. Furthermore, methods have been proposed to quantify uncertainty to account for variability in modal testing of the SNL research blades.^{15–17} In one instance, for a free–free analysis, the variability of test results is quantified to account for the support conditions, mass loading of the accelerometers, cable effects on the free–free condition and temperature of the ambient environment. In addition, natural variability is considered to investigate the repeatability of measured natural frequencies from one test specimen to another. The results from these studies help to quantify sources of uncertainty (relative to each other) and provide important considerations for the free–free modal testing of wind turbine blades.

It is important to propose a robust methodology to develop FE models because as previously observed, there can be variability during experimental testing of wind turbine blades that will result in slightly different responses.¹⁵ In addition to variation among the blades, further variation will result because of the experimental campaigns (calibration errors, test-to-test variability, etc.), hence requiring even more robustness in the analysis. This publication and its companion second part propose such methodology that accounts for the experimental variability, numerical uncertainty and modeling uncertainty introduced, for example, by the lack of knowledge in constitutive material properties.

3. DERIVATION OF AN UPPER BOUND OF SOLUTION UNCERTAINTY

Because numerical uncertainty is an essential part of our quantification effort for V&V, we start by proposing an upper bound of solution uncertainty on the basis of the concept of asymptotic convergence. The upper bound arrived at is compared with the well-known grid convergence index (GCI) of Roache¹⁸ and used in Section 6 to select an appropriate mesh size.

3.1. Derivation on an upper bound of solution uncertainty

The partial differential equations solved by a numerical method, such as a FE software, always provide an approximation of the ‘exact-but-unknown’ solution of the continuous equations. Such an approximation comes in two steps, according to the formalism established by the Lax equivalence theorem.¹⁹ Convergence states that the code *self-converges* to a solution denoted by the symbol y^* , or ‘ $y(\Delta x) \rightarrow y^*$ ’, as the level of resolution in the calculation increases. Consistency of the numerical method, on the other hand, provides ‘ $y^* \rightarrow y^{\text{Exact}}$ ’. For simple test problems, the unknown solution y^* can be obtained from modified equation analysis (MEA), as explained in Hirt²⁰ and Warming and Hyett.²¹ The distinction between solutions y^* and y^{Exact} emphasizes that a code could potentially self-converge to a solution that is different from the exact solution.

For practical applications that involve complicated geometries, boundary conditions or forcing functions, the exact solution y^{Exact} cannot be derived in closed form. Likewise, MEA becomes intractable, which prevents the derivation of the solution y^* . Our purpose, therefore, is to bound the difference $|y^* - y(\Delta x)|$. For a consistent numerical method, and in the limit of asymptotic convergence, the discrete solutions $y(\Delta x)$ converge to the solution y^* of the modified equation, which in turn reduces to the exact-but-unknown solution y^{Exact} as $\Delta x \rightarrow 0$. Because these solutions are ‘equal’ only in the asymptotic limit, we seek an upper bound of solution error defined as

$$|y^* - y(\Delta x)| \leq U(\Delta x) \cdot |y(\Delta x)| \quad (1)$$

In the application of Section 5, y^* denotes the best-possible estimation of an ‘exact-but-unknown’ natural frequency, whereas $y(\Delta x)$ is the approximation obtained by running the calculation at mesh size Δx .

A solution for the upper bound $U(\Delta x)$ can be derived by examining the relationships between the discrete solutions resulting from a coarse-mesh (Δx_C) and a fine-mesh (Δx_F) discretization. If the resolutions Δx_C and Δx_F provide discrete solutions within the regime of asymptotic convergence, the following (approximate) equations can be postulated:

$$y^* \approx y(\Delta x_F) + \beta \cdot \Delta x_F^p \quad \text{and} \quad y^* \approx y(\Delta x_C) + \beta \cdot \Delta x_C^p \quad (2)$$

where β is a pre-factor coefficient and the exponent p denotes the rate of convergence. This formalism derives from MEA, as mentioned previously.²¹ MEA defines a Taylor series-like expansion that is usually infinite and whose sophistication depends on the combination of partial differential equations solved and properties of the numerical method implemented.

Equations (2) are simple approximations of the MEA where the higher-order terms are ignored, the pre-factor β is assumed to be constant (which is generally not the case), convergence is monotonic as $\Delta x \rightarrow 0$, and analysis is restricted to scalar-valued quantities (Hemez²² offers a generalization to one-dimensional curves or multidimensional fields). These assumptions translate the fact that truncation effects (caused by mesh discretization) dominate the overall production of numerical error within the regime of asymptotic convergence. It can be observed that if expressed on a logarithmic scale, equations (2) define a linear relationship between the errors and mesh sizes. The slope of this linear relationship (or exponent p) provides the order of accuracy of the numerical method.

An elementary rearrangement of the well-known triangular inequality $|a| + |b| \geq |a + b|$ produces the form $|c - d| \geq |c| - |d|$. (Simply substitute $c = a + b$, $d = b$.) From this, using the quantities

$$c = y(\Delta x_C) - y^* \quad \text{and} \quad d = y(\Delta x_F) - y^* \quad (3)$$

combined with equations (2) and incorporating the assumption that convergence is monotonic (such that the sign of the pre-factor coefficient β can be kept constant), results in

$$|y(\Delta x_C) - y(\Delta x_F)| \geq |y^* - y(\Delta x_C)| - |y^* - y(\Delta x_F)| \approx \beta \cdot \Delta x_C^p - \beta \cdot \Delta x_F^p \quad (4)$$

Using the mesh refinement ratio defined as $R = \Delta x_C / \Delta x_F > 1$, equation (4) becomes

$$|y(\Delta x_C) - y(\Delta x_F)| \geq \beta \cdot \Delta x_F^p \cdot (R^p - 1) \quad (5)$$

Inserting the first one of equations (2) to replace the term $\beta \cdot \Delta x_F^p$ in equation (5), we arrive at

$$|y(\Delta x_C) - y(\Delta x_F)| / (R^p - 1) \geq |y^* - y(\Delta x_F)| \quad (6)$$

This final equation is the upper bound sought. When the exact solution y^{Exact} of the continuous equations is unknown, which is generally the case of a general-purpose FE calculation, one can no longer talk of an ‘error’. The difference $|y^* - y(\Delta x)|$ in the right-hand side of equation (6) becomes an *uncertainty* because of truncation effects. The best that one can achieve is to bound this uncertainty at any given level of mesh resolution Δx .

3.2. Analogy to the grid convergence index

Our proposal for an upper bound $U(\Delta x)$ of solution uncertainty at mesh resolution Δx is

$$U(\Delta x) = \frac{|y(R \cdot \Delta x) - y(\Delta x)|}{(R^p - 1)} \quad (7)$$

where Δx is a characteristic mesh size of the calculation and R denotes the refinement ratio (where, by definition, $R > 1$). It is emphasized that definition (7) only requires two calculations at the coarse and fine levels of mesh resolutions $\Delta x_C = R \cdot \Delta x$ and $\Delta x_F = \Delta x$, respectively.

This definition is analogous to the GCI of Roache,^{12,18} defined as

$$GCI(\Delta x) = \frac{F_S}{(R^p - 1)} \left| \frac{y(R \cdot \Delta x) - y(\Delta x)}{y(\Delta x)} \right| \quad (8)$$

where F_S denotes the so-called ‘safety factor’ added to provide conservatism and generally chosen within the range $1 \leq F_S \leq 3$. Clearly, the upper bound (7) of solution uncertainty is related to the GCI by the following equation where $F_S = 1$:

$$U(\Delta x) = GCI(\Delta x) \cdot |y(\Delta x)| \quad (9)$$

Even though the definitions are similar, modulo $F_S = 1$, it is emphasized that the motivation put forth by P.J. Roache is different. The GCI is explained by Roache¹⁸ as

The idea behind the proposed GCI is to approximately relate the ϵ [...] obtained by whatever grid convergence study is performed (whatever p and r) to the ϵ that would be expected from a grid convergence study of the same problem with the same fine grid using $p = 2$ and $r = 2$, i.e., a grid doubling with a second-order method.

This explanation justifies the choice of a safety factor $F_S = 3$ to cancel out the $(R^p - 1)$ term in equation (8). This renders the GCI of an arbitrary mesh refinement study comparable with a value obtained with $R = 2$ (grid doubling) and $p = 2$ (second-order accurate method).

To the best of the authors’ understanding, the GCI was not proposed initially as an attempt to define an upper bound of solution uncertainty. Equation (9) sheds new light on an index that can be used to estimate where the ‘exact-but-unknown’ solution y^* may be located relative to a discrete solution obtained by analyzing the problem with a level of mesh resolution Δx . This is analogous to statistics obtained from physical observations, such as a mean value, that come with an uncertainty that estimates the unknown value of the experimental setup. The upper bounds of solution uncertainty presented in Section 5 are based on equations (8–9) with $F_S = 3$.

4. CODE VERIFICATION ACTIVITIES

Code verification is the first step of the V&V study. ‘Spot check’ verification is performed to assure that the FE software is running properly, without any significant programming mistake that would negatively impact the results sought. One specific area of concern is that in the past, shell elements have been found to have shortcomings in torsion.¹⁰ Because the first torsion of the wind turbine blade is of interest, this potential issue warrants careful investigation.

To verify the correctness of implementation of shell elements in ANSYS, together with their numerical performance, a simple hollow cylinder with known analytical solution is modeled. (This, by design, hews closely to the modeling performed in Laird *et al.*¹⁰) ANSYS version-12.1 is used to model and analyze this code verification test problem for which three scenarios are explored: (i) a bending load applied to a fixed-free cylinder; (ii) a torsion load applied to the same fixed-free cylinder; and (iii) the modal analysis of a fixed-fixed cylinder. These three scenarios feature the same geometry with different cases of loading and boundary condition.

The varying boundary conditions are explored to assess the ability of the code to predict more than one configuration. In addition to the fixed-free boundary, a fixed-fixed setup is exercised because implementing a fixed boundary is somewhat more complicated and, therefore, prone to potential mistakes in the analysis software.

4.1. Verification of the bending stress

The bending stress is verified by reporting results from the shell elements at midsection where there is no membrane-bending coupling. The closed-form solution for the bending stress is

$$\sigma = \frac{M \cdot c}{I} \quad (10)$$

where σ denotes the maximum normal stress due to bending, M is the bending moment, c is the greatest distance from the neutral axis and I represents the cross-sectional moment of inertia.

Figure 1 illustrates one of the meshes analyzed where the bending load is applied. The vertical, upward-pointing arrows indicate the location and direction of the applied load. The analysis of the same test problem is repeated with increasing levels of mesh resolution. Figure 2 shows the solution error as a function of mesh size. The percentages of solution error are depicted on the left, and the asymptotic convergence of numerical solutions is illustrated on the right.

It can be observed from Figure 2 that as expected, the solution error decreases as a function of mesh resolution. A model with fewer than 1000 elements produces less than 1% error between the predicted bending stress and analytical solution of equation (10). In addition, the log-log representation indicates that solution error converges with a rate of convergence of $p = 2.17$. This observation matches expectation because quadratic shell elements, which are expected to produce an accuracy of $p^{\text{Theory}} = 2$, are used for discretization. It is concluded that the element is implemented correctly and performs according to expectation to model the response under bending load.

An inspection of asymptotic convergence in Figure 2 (right) reveals that the convergence is not quite monotonic. Solutions produced by the two finest meshes actually have greater errors than any of the next three solutions obtained with coarser meshes. The reasons for these oscillations are not apparent, although it is suspected that such effects owe to either round-off errors or finite elements demonstrating uncharacteristic behavior at sufficiently small sizes. Because our analysis searches for overall trends using simple power laws, such as the best-fitted model $\log(|\sigma^* - \sigma(\Delta x)|) = 2.17 \cdot \log(\Delta x) - 0.61$ illustrated in Figure 2 (right), we believe that our conclusions are not adversely affected by this erratic behavior.

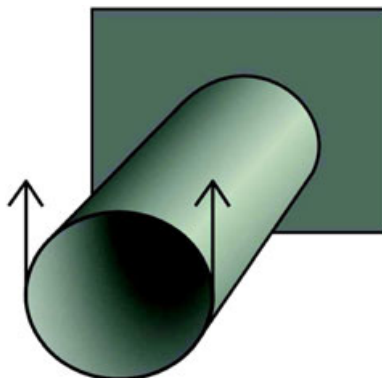


Figure 1. Definition of the hollow cylinder-in-bending test problem.

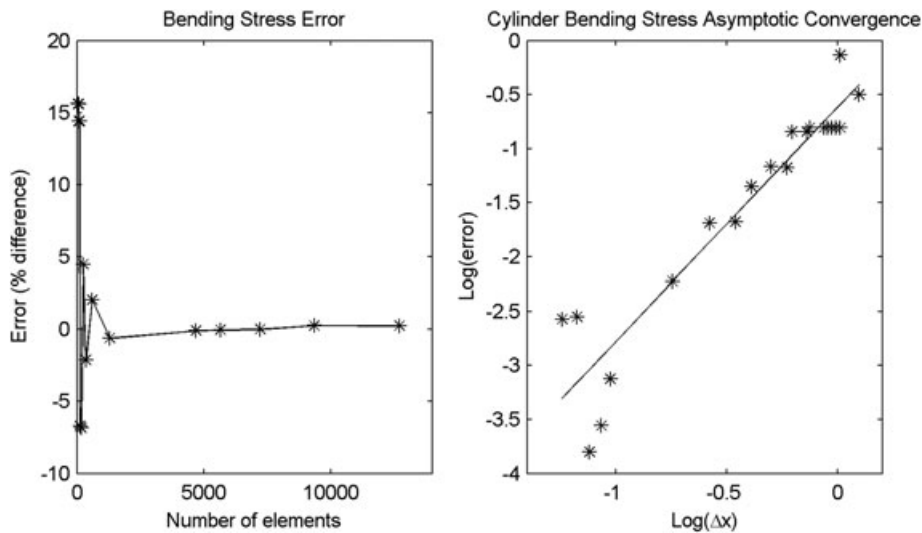


Figure 2. Solution error (left) and asymptotic convergence (right) of the bending problem.

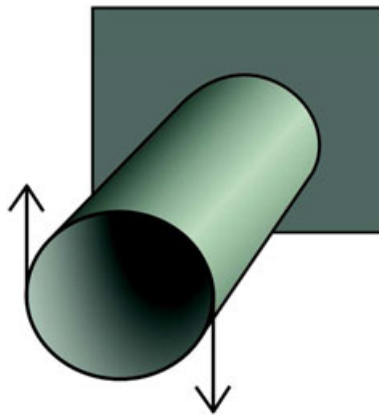


Figure 3. Definition of the hollow cylinder-in-torsion test problem.

4.2. Verification of the shear stress

A similar analysis is performed for the case of a torsion load. The closed-form solution is

$$\tau = \frac{T \cdot r}{J} \quad (11)$$

where τ denotes the maximum shear stress due to torsion, T is the torque applied, r is the outer radius of the cylinder and J represents the polar moment of inertia.

Figure 3 illustrates the test problem where the applied load is indicated by opposite-pointing arrows that define the torsion. The overall evolution of solution error as a function of mesh resolution is depicted in Figure 4.

As noted previously, it can be observed from Figure 4 that fewer than 1000 finite elements are needed to reach less than 1% error between the predicted shear stress and analytical solution of equation (11). The log–log representation leads to an observed rate of convergence of $p = 2.05$. Also noticeable is the stable behavior of the shell element in torsion, as indicated by a solution error that is more predictable than the error in bending (Figure 3 (right)) as the mesh resolution is refined. These observations are strong evidence that the shell element implemented in ANSYS performs according to expectation of second-order accuracy to model the response under both bending and torsion loads.

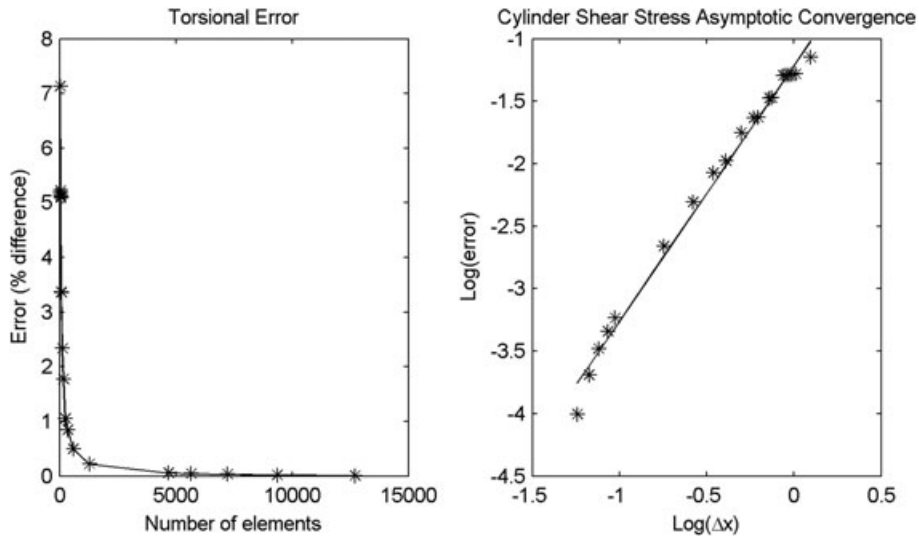


Figure 4. Solution error (left) and asymptotic convergence (right) of the torsion problem.

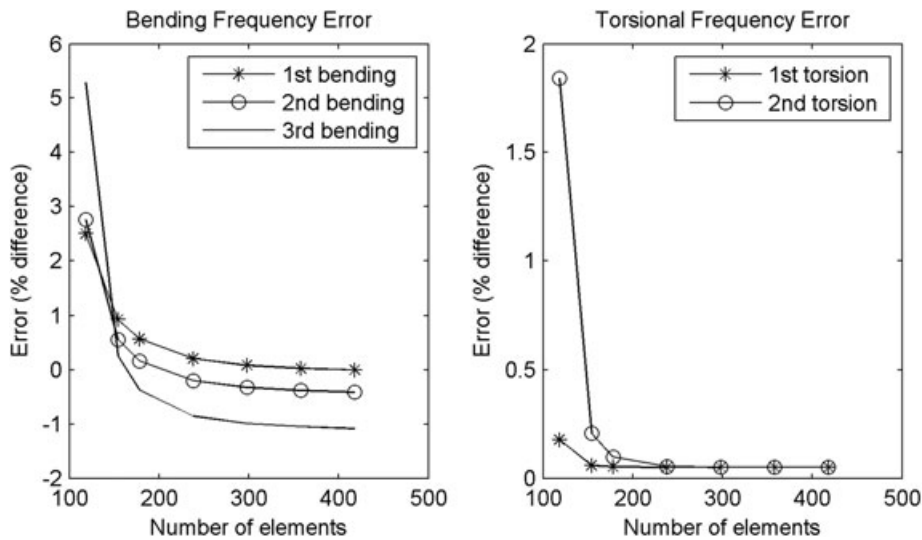


Figure 5. Solution errors for bending (left) and torsion (right) natural frequencies.

4.3. Verification of the modal solution

Because the FE model is ultimately used to simulate the vibration response of a wind turbine blade, the ability of the ANSYS shell element to reach an accurate modal solution also needs to be verified. A third test problem is analyzed to simulate the vibration of a simply supported, hollow cylinder without axial constraint. Highly accurate approximations of the natural frequencies of vibration are obtained from Blevins²³ and used as substitutes to the ‘exact-but-unknown’ solutions. Figure 5 plots the relative frequency errors in bending and torsion as a function of Δx .

Figure 5 (left) indicates that fewer than 100 elements suffice to predict the first three bending frequencies of the hollow cylinder to within 1% error or less. Figure 5 (right) shows that a finer mesh with 250 elements converges to less than 0.1% error, confirming the ability of the shell elements to predict the torsion frequency.

Figure 6 shows the agreement between simulated (left) and closed-form (right) mode shapes for the first three bending modes. The figure illustrates the excellent level of correlation with which mode shape deflections are predicted. This observation increases confidence in the ability of the FE model to accurately capture the bending of the main spar cap of the wind turbine blade.

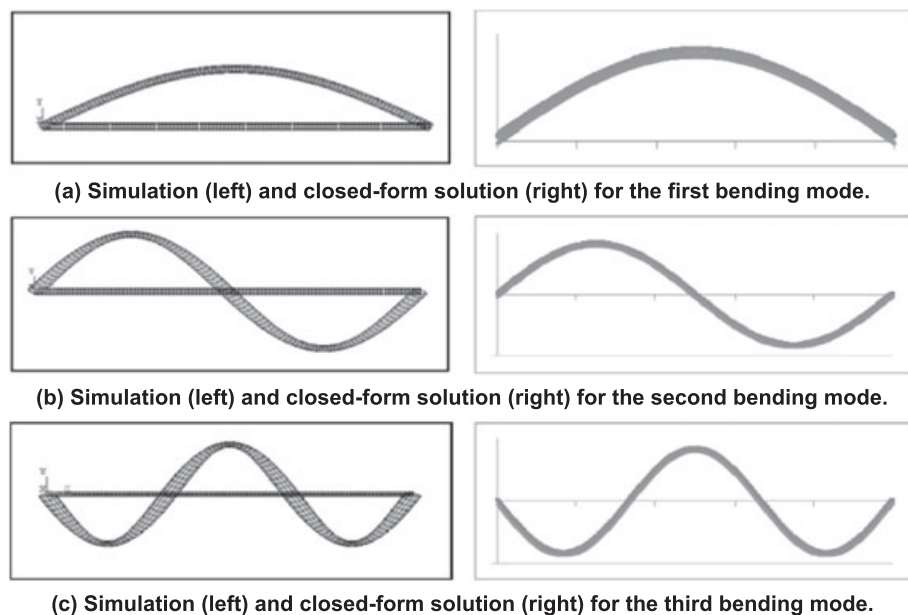


Figure 6. Comparison of simulation and closed-form mode shape deflections.

4.4. Verification of the pre-processing software NuMAD

After satisfactorily checking the quality of the ANSYS software, it is next desired to perform accompanying code verification studies of the NuMAD pre-processor, developed by SNL to ease the production of FE models of wind turbine blades. This software receives information of cross-sectional geometry at each station and material properties for each section comprising the structure. It produces a text file (written in ANSYS parametric design language) that defines an ANSYS model corresponding to these characteristics.

To verify the suitability of a NuMAD-generated model, the cylinders created in Sections 4.1 and 4.2 are recreated with NuMAD. The main difference is that constraint equations are imposed for all nodes at the tip, or free, end of the blade so that the shape cannot be deformed. However, the material properties are stiff enough in the unconstrained, ANSYS-based setup that effects of this change never become apparent. Mesh refinement is performed to assess the performance of the NuMAD-generated model for bending and shear stresses.

The results are similar to those obtained previously. As an alternative illustration of the convergence upon the true solution, Figure 7 shows the bending and torsional stress solutions when solved by ANSYS using the NuMAD pre-processor. The analysis uses the GCI to describe the bounds of solution uncertainty due to truncation error (see equations (8–9) of Section 3). Stress values and uncertainty bounds are shown in Figure 7 as a function of element size. The upper bounds function as expected: the exact solutions of equations (10) for bending and (11) for torsion are converged upon as the element size is refined. Even though not indicated by Figure 7, it is also verified that for larger element sizes, the upper bounds always contain the exact solutions.

Figure 7 indicates that one significant difference between bending (left) and torsion (right) is that asymptotic convergence is monotonic in the latter case, hence producing one-sided bounds of solution uncertainty. On the other hand, convergence of the bending stress is oscillatory, which leads to two-sided bounds of uncertainty since the two cases ' $y(\Delta x) \geq y^*$ ' and ' $y^* \geq y(\Delta x)$ ' are possible as $\Delta x \rightarrow 0$. On the basis of the agreement between the exact and discrete solutions for the NuMAD-created cylinder test problem, it is deemed satisfactory that the pre-processing software accomplishes the basic function it purports to do.

5. EXPERIMENTAL MODAL ANALYSIS OF THE WIND TURBINE BLADE

At this point of the study, the ANSYS code for FE modeling and its pre-processor software NuMAD have undergone sufficient code verification activities for the purpose intended. A model of the CX-100 wind turbine blade is generated, as described in Section 6. One lingering question in the development of the FE model is the selection of an appropriate

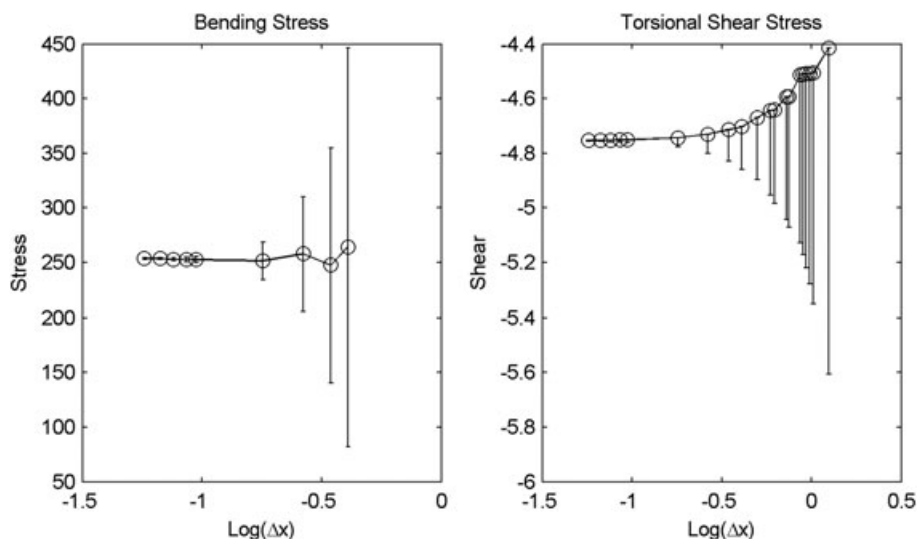


Figure 7. Solutions for bending (left) and torsion (right) stress, with uncertainty bound.

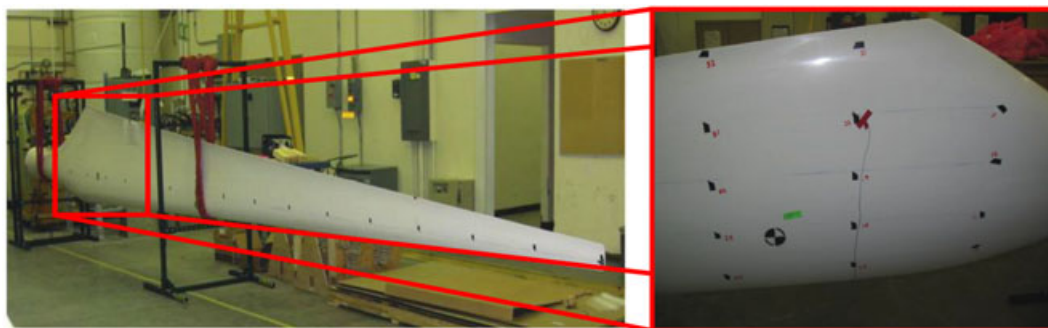


Figure 8. Free-free modal testing configuration (left) and close-up of excitation grid (right).

mesh size for the calculations. This question refers to the level of discretization needed to support sensitivity analysis and uncertainty quantification.⁷

Modal testing of the CX-100 blade is performed under free-free and fixed-free boundary conditions at Los Alamos National Laboratory (LANL). These measurements are used not only to calibrate parameters of the simplified model as explained in Van Buren *et al.*⁷ but also to guide the choice of an appropriate level of mesh resolution. This is a significant departure from the common V&V paradigm that tends to promote a strict separation between code verification activities and comparison between predictions and measurements. It is emphasized that only the experimental *variability*, and not the measured response, is used.

Testing includes exploring the overall levels of experimental variability that result from using different setups where excitation locations, excitation types and support conditions are varied to quantify their potential effects on system identification. Roving impact hammer test is performed to collect modal data with uniaxial accelerometers at three locations on the blade. A linear average with five repeats and a 150 Hz sampling frequency is used. The acceleration response is measured for 11 s. No window function is applied because of the relatively long sampling period. Figure 8 depicts one of the setups tested (left) and shows a close-up of the grid used to record locations used for excitation and sensing (right). Van Buren *et al.*⁷ discussed the effect that varying these configurations has on the identification of resonant mode shapes and natural frequencies, in comparison with corresponding predictions of the FE model.

The experimental investigation also includes performing linearity and reciprocity checks to verify the quality of datasets collected. A linearity check consists of testing the CX-100 blade with increasing levels of force excitation. A structure that responds linearly, which is a fundamental assumption of the system identification method used to extract the resonant modes, should yield similar frequency response function (FRF) curves regardless of the applied force. A reciprocity check

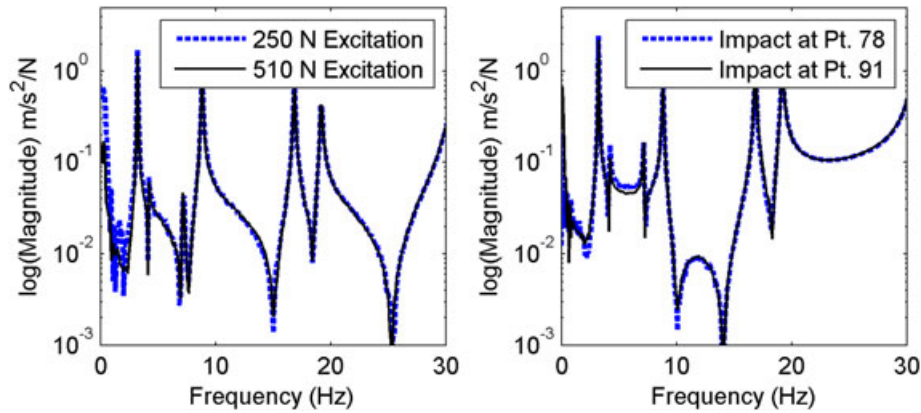


Figure 9. Verification of linearity (left) and reciprocity (right) during modal testing.

Table I. Statistics of system identification obtained for the CX-100 blade.

Type of mode	Mean statistic (Hz)	Standard deviation (Hz)	Variability ^a (%)
First flap-wise bending	7.617	0.004	0.06
Second flap-wise bending	20.167	0.055	0.27
Third flap-wise bending	32.256	0.051	0.16

^aThe coefficient of variance listed in the last column is defined as the standard deviation (third column) divided by the mean (second column). These statistics are based on 27 replicates for the free-free vibration tests.

consists of swapping pairs of excitation and sensing locations to compare FRF curves. Another assumption of linear structural dynamics is that the load path from point A to point B is identical to the reverse path. Establishing that the FRF curves are, again, similar verifies the assumption of reciprocity.

Figure 9 illustrates that for these series of modal tests, the CX-100 blade behaves as a linear structure and exhibits reciprocity. The FRF curves compared on the left originate from modal tests performed with different levels of force excitation. It is observed that their agreement is excellent. Likewise, the curves compared on the right of Figure 9 originate from a reciprocity test at two locations, and the same conclusion is reached. The reader is referred to Deines *et al.*²⁴ to learn further details about the experimental setup and results of these vibration tests.

The levels of variability observed are quantified and listed in Table I, summarizing results for testing the blade with free-free boundary conditions. Overall, very low levels of variability are obtained, which are due to replicated modal tests on the same wind turbine blade. This quantification of experimental variability does not account for specimen-to-specimen variability, experimenter variability or test setup repeatability. These results are also used in the companion publication as ‘baseline’ for inference of the idealized material properties of the FE model.⁷

Besides providing important information for test-analysis correlation, the statistics of Table I are also used to guide the selection of a mesh size Δx at which the subsequent parametric studies (sensitivity analysis, inference uncertainty quantification, etc.) are conducted. The maximum level of experimental variability observed is 0.27% for the second free-free bending mode.

Since this value corresponds to one standard deviation σ , the $\pm 3\sigma$ (two-sided) bounds are equal to 1.62% variability. These $\pm 3\sigma$ bounds are adopted to characterize the experimental variability since they account for 98% of the total probability mass, assuming a Gaussian probability law. This choice yields a fair comparison with the bounds of total solution uncertainty quantified in Section 6.2, where the mesh size is chosen such that the numerical uncertainty is similar to this 1.62% variability for predictions of the resonant frequencies.

6. SOLUTION VERIFICATION AND QUANTIFICATION OF NUMERICAL UNCERTAINTY

This section starts by describing attributes of the FE model developed to simulate bending deformation shapes of the CX-100 wind turbine blade. The main assumption that enables fast-running calculations, namely the use of homogenized material properties, is proposed. Solution verification is carried out, first, to assess the numerical performance of the model

and, second, to choose a mesh resolution that results in an appropriate level of numerical uncertainty. Finally, the behavior of the NuMAD pre-processing software is revisited to assure that its mesh sensitivities do not produce adverse consequences for the FE model developed.

6.1. Development of a simplified model of the CX-100 blade

The model of the CX-100 blade is developed with the NuMAD pre-processor and imported into the ANSYS software. The blade is 9 m long, and its geometry is represented in the model using design specifications with as few simplifications as possible. Figure 10 provides a comparison of the simplified FE model used in this study to a high-fidelity FE model, which can more accurately capture the taper of materials used to define the root section.

The model used in this study is achieved by segmenting the geometry of the blade into a small number of sections and defining smeared properties for each section. This is carried out, in contrast to the type of modeling provided in Figure 10, because a high-fidelity model is computationally too expensive to lend itself to the parametric studies that we wish to pursue. It is emphasized that the number and definition of smeared sections are considered to be a model-form choice, as opposed to a discretization, which implies that the ‘convergence’ of the vibration response as a function of the number of sections is not currently studied. The ability of the simplified model to predict the bending modes of vibration with reasonable accuracy is discussed in Van Buren *et al.*⁷

Six sections are defined: the shear web, root, spar cap, trailing edge, leading edge with balsa and leading edge without balsa. Figure 11 represents five of these sections, whereas the interior shear web is illustrated in Figure 12. To reflect the tapering of the edges in the real-life structure, the trailing edge and leading edge of the blade are further subdivided into three subsections of differing stiffness coefficients.

Within each section, an isotropic material is defined by assuming smeared cross-sectional properties. The validity of this simplification is explored in Van Buren *et al.*⁷ by performing sensitivity analysis, uncertainty quantification and comparisons between model predictions and physical measurements. The rule of mixtures is utilized to homogenize the composite

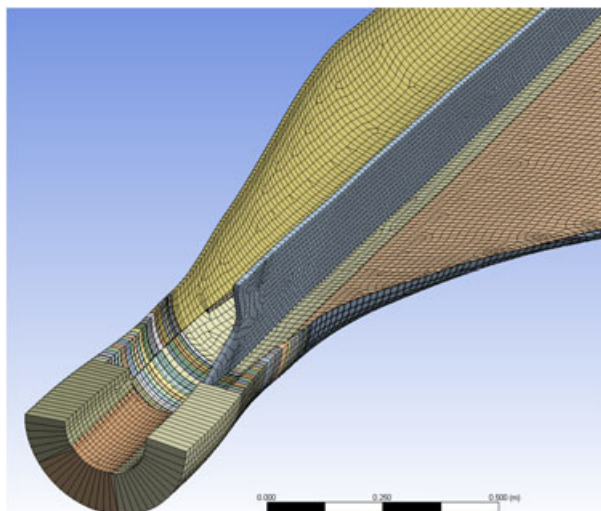


Figure 10. High-fidelity CX-100 ANSYS model with detailed cross-sectional modeling.

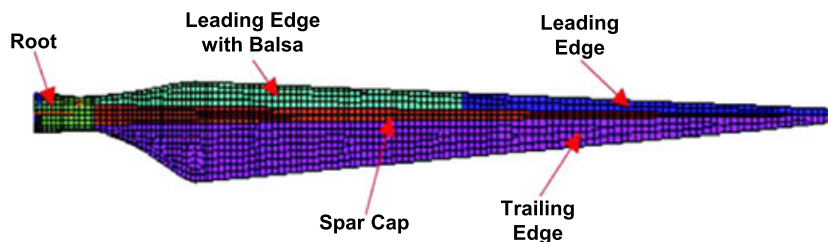


Figure 11. Illustration of the ANSYS model showing different sections of the blade.

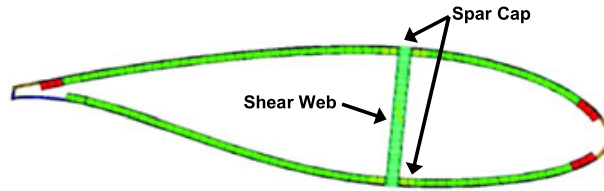


Figure 12. Illustration of the ANSYS model's shear web located inside the blade.

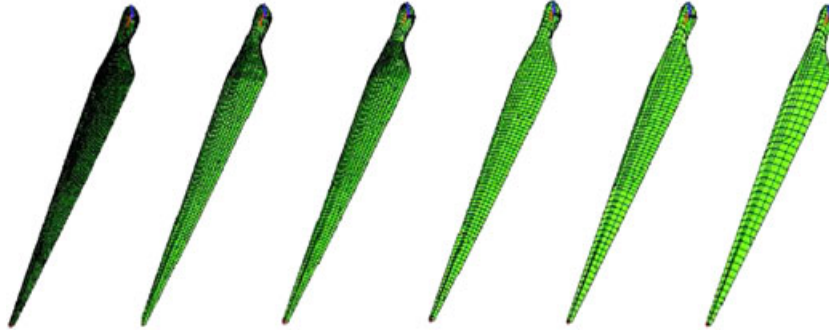


Figure 13. Six meshes used to assess the asymptotic convergence of vibration modes.

cross sections.²⁵ On the basis of the structure of composites, the rule of mixtures blends together the differing material properties and estimates the material property of an equivalent isotropic material.

One important aspect of performing numerical simulations is to assess if the equations of motion, or conservation laws, are discretized with enough resolution to produce 'good-quality' numerical solutions. A mesh convergence study is performed to verify the performance of the ANSYS software, as applied to the CX-100 blade model, and determine an appropriate level of mesh resolution for the calculations. Our decision criteria are to, first, reach a level of numerical uncertainty that is comparable with, or smaller than, the overall experimental variability, while also being capable to run a linear, modal extraction on a PC platform in fewer than 60 s.

6.2. Mesh refinement and quantification of truncation error

After having scripted and automated the execution of the FE model, over 20 meshes are analyzed to predict the low-order resonant modes. Figure 13 illustrates six of these calculations, where the figures from left to right show progressively lower levels of mesh resolution. Figure 14 reports the values of predicted resonant frequencies as a function of mesh size. The three natural frequencies shown are the three modes targeted: first, flap-wise bending (mode 1); second, flap-wise bending (mode 3); and third, flap-wise bending (mode 4). It is clear from the figure that these resonant frequencies exhibit a satisfactory degree of convergence as the number of elements of the discretization increases.

The numerical uncertainty due to truncation error, that is, lack of resolution in the calculation, is bounded as explained in Section 3 for the three bending frequencies of interest. These upper bounds are defined as

$$\left| \frac{\omega^* - \omega(\Delta x)}{\omega(\Delta x)} \right| \leq U(\Delta x) \quad (12)$$

where ω^* is the best-possible estimation of the 'exact-but-unknown' frequency whereas $\omega(\Delta x)$ is the approximation obtained by running the calculation at mesh resolution Δx . The uncertainty bound $U(\Delta x)$ is related to the GCI through the introduction of a safety factor F_S , as illustrated in equations (8) and (9). When the solution ω^* is estimated, for example, through the method of Richardson's extrapolation, it is possible to examine the solution error and assess asymptotic convergence.¹² This extrapolation scheme leads to an approximation obtained simply as

$$\omega^* \approx \omega(\Delta x) + \frac{\omega(\Delta x) - \omega(R \cdot \Delta x)}{R^p - 1} \quad (13)$$

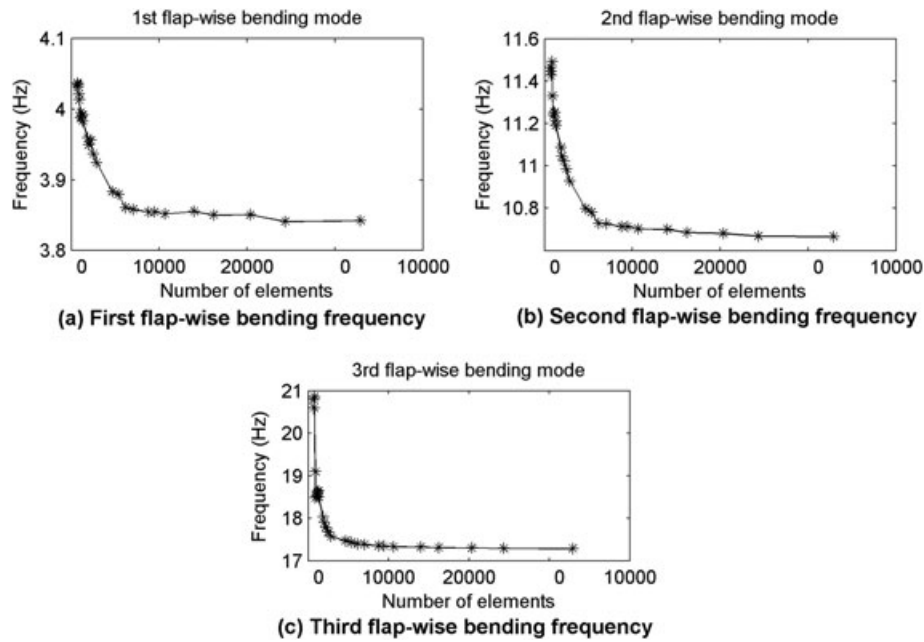


Figure 14. Convergence of resonant frequencies as a function of mesh resolution.

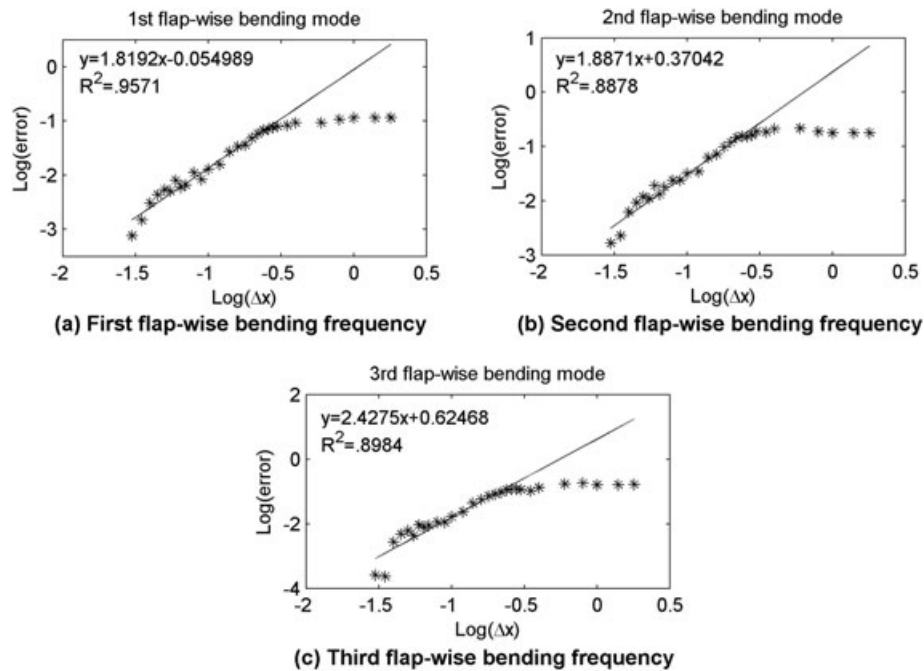


Figure 15. Asymptotic convergence of frequencies as a function of mesh resolution.

Figure 15 illustrates the behavior of solution error $|\omega * -\omega(\Delta x)|$ as a function of mesh size Δx for the same three modal frequencies as those of Figure 14, where the exact solution is approximated by applying equation (13) to the two finest levels of mesh resolution.

Convergence is observed even though five to seven models analyzed with the coarsest levels of resolution are located in a non-asymptotic region where refining the mesh does not necessarily decrease the truncation error. These under-resolved calculations are disregarded for the purpose of best-fitting the model of truncation error $|\omega * -\omega(\Delta x)| = \beta \cdot \Delta x^p$, whose

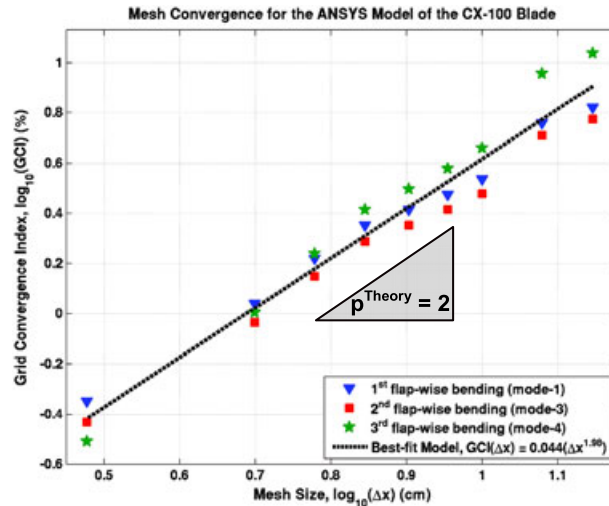


Figure 16. Values of the grid convergence index for the first three flap-wise bending modes.

definition applies only within the asymptotic regime of convergence. The log–log scale of Figure 15 indicates that convergence is nearly second order for the models located in the asymptotic regime. This is confirmed by a quantitative analysis that best fits the two unknowns (β ; p) of simple power-law equations $|\omega * -\omega(\Delta x)| = \beta \cdot \Delta x^p$ to the error data of Figure 15. The observed rates of convergence are equal to $p = 1.82$ for the first flap-wise bending mode, $p = 1.89$ for the second flap-wise bending mode and $p = 2.43$ for the third flap-wise bending mode. It implies that second-order accuracy is achieved for the modal analysis.

Figure 16 shows the GCI obtained with a safety factor of $F_S = 3$. Three bending frequencies are denoted by different symbols. The dashed line illustrates the goodness-of-fit obtained with a simple power-law equation $GCI(\Delta x) = \beta \cdot \Delta x^p$ for the average GCI. Best-fitted coefficients equal to $\beta = 0.044$ and $p = 1.98$ lead to, again, strong evidence of second-order accuracy. On the basis of these observations, the hypothesis that the finest levels of mesh resolution provide solutions within the regime of asymptotic convergence cannot be rejected.

So far, the mesh refinement results have been analyzed to assess the performance of the FE software. Although observing second-order accuracy is reassuring, it may not be of great practical interest given that the code verification activities of Section 4 have already concluded to the lack of significant implementation issue for the intended purpose. It is, however, a first step needed to support the quantification of solution uncertainty. What is more valuable to the practicing engineer is to select an appropriate mesh size to pursue the parameter studies of Van Buren *et al.*⁷

Often, the strategy to select a mesh size is ‘run as fine a mesh as computationally feasible’. This approach may lead to a waste of resources when the resolution employed is too fine. It is also unsatisfactory in the context of V&V because this rationale does not take into account the intended purpose of the numerical simulation, desired level of prediction accuracy and overall reproducibility of experimental testing (whenever available). In this work, an alternative strategy is proposed on the basis of the overall level of experimental variability. While challenging the conventional separation between verification and test-analysis correlation, our proposal offers the advantage of avoiding to select a mesh size in a ‘vacuum’.

Our guiding principle is to use a mesh discretization that provides an overall level of numerical uncertainty comparable with the experimental variability. The rationale is that there is no reason to provide significantly more prediction accuracy than the level with which the response can be measured when experimental testing is replicated.

Table II lists the GCI of equation (8) obtained with a safety factor of $F_S = 2$. This choice is made, instead of $F_S = 3$ used in Figure 16, by analogy to the $\pm 3\sigma$ bounds of experimental variability of Section 5 that are two sided. Our contention is to select a mesh size that leads to a numerical uncertainty similar to the 1.62% level of experimental variability. Another constraint imposed by the parameter studies is to minimize time to solution. The 7 cm mesh, although it satisfies the first criterion, does not provide modal solutions in fewer than 60 s on our PC computing platform (Intel single-core, 2 GHz processor, 4 GB memory, Windows 7 operating system). It is decided that the next level of mesh size provides the best *trade-off* between the two competing constraints. The solution uncertainty obtained at $\Delta x = 8$ cm is the fourth row highlighted in bold in Table II. The 8 cm mesh calculates modal solutions in fewer than 60 s while yielding 1.78% solution uncertainty, on average, which meets the objective of comparing favorably with the $\pm 3\sigma$ bound of 1.62% variability assessed from Table I.

Table II. Grid convergence index (GCI) for predictions of the three bending modes of interest.

Mesh size, Δx (cm)	First mode GCI (%)	Third mode GCI (%)	Fourth mode GCI (%)	Mean GCI (%)
5.0	0.77	0.61	0.67	0.68
6.0	1.11	0.94	1.16	1.07
7.0	1.50	1.29	1.73	1.51
8.0	1.73	1.50	2.10	1.78
9.0	1.99	1.73	2.53	2.08
10.0	2.30	2.01	3.06	2.46

These calculations are based on a constant safety factor, $F_S = 2$; see equation (8).

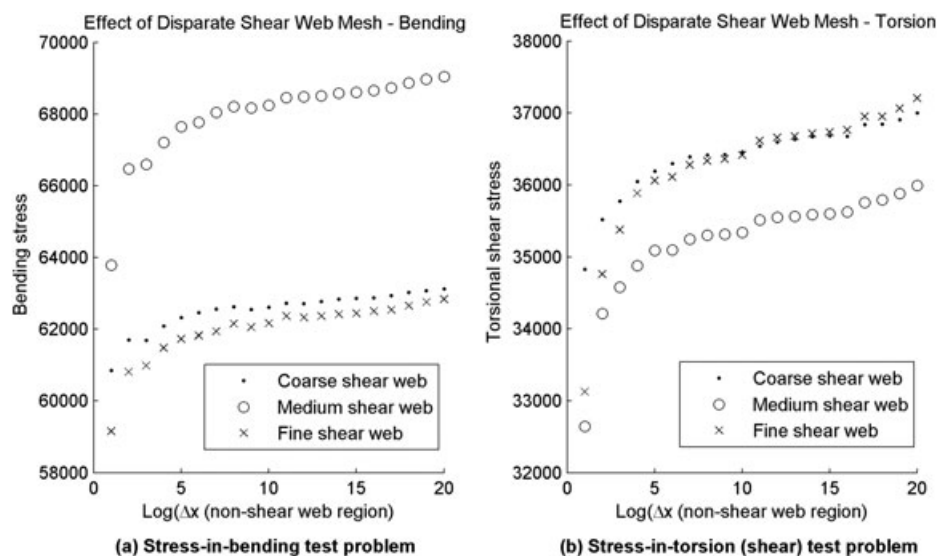


Figure 17. Stress values for different meshing options of the shear web.

To pursue the parameter studies of Van Buren *et al.*,⁷ the decision is made to ‘freeze’ the resolution at $\Delta x = 8$ cm. It gives a FE model with 3070 elements from which the resonant modes can be extracted in 60 s, approximately.

6.3. Mesh sensitivity introduced by the pre-processing software NuMAD

Through the course of the above analyses, several other variables are altered to explore their potential effects upon the truncation error. Notably, it is attempted to explore different meshes by overriding the default meshing method implemented by the pre-processor NuMAD and assign a coarser or finer mesh to the shear web than the resolution used for the other structural components of the CX-100 model. This study involves creating and running a separate post-processor to modify the output generated by the NuMAD software.

Figure 17 illustrates qualitative results for a bending stress analysis and a torsional shear stress analysis, using three different options of shear web meshing—a coarse, medium and fine mesh (as compared with the other components of the model). The values of stress are depicted as a function of mesh size for the other, non-shear-web elements. Our hypothesis is that there is no reason to observe any significant cross-sensitivity between the mesh size used to discretize the shear web and the mesh size used to discretize the other components.

The results yield some surprising findings: in neither case is the effect of the mesh size of the shear web on the resulting stress monotonic. The predictions obtained with the medium mesh size for the shear web are, in each case, extreme, when they instead would be expected to lie between predictions obtained with the coarser and finer levels of resolutions. The calculations exhibit the expected behavior at any given level of shear web resolution, that is, moving along one of the datasets as $\Delta x \rightarrow 0$. What is unexpected is to observe the extent to which predictions are sensitive to the combination of mesh sizes for the shear web and other components.

No explanation for this effect is readily apparent. These observations are nevertheless made in the interest of full disclosure of the results obtained. For all results other than those discussed in this section, FE models are generated from the

default, homogeneous mesh option of the pre-processor. The mesh cross-sensitivity observed is therefore not believed to be detrimental to the quality of our numerical predictions.

7. CONCLUSION

This publication discusses the development of a FE model for the CX-100 wind turbine blade and overviews some of the analysis procedures implemented to verify the code, quantify the overall level of solution uncertainty due to truncation error and compare it with experimental variability. These are some of the activities typically deployed in a V&V study. Other activities that include sensitivity analysis, the propagation of parametric uncertainty from inputs of the model to its predictions and the calibration of model parameters are addressed in a companion paper for the same application.⁷

To rigorously quantify numerical uncertainty in the absence of an exact solution to the equations of motion, or conservation laws, being solved, an upper bound of solution error is derived. An analogy is made with the well-known GCI when a specific value of its safety factor is implemented. Another novelty of this publication is to propose a criterion based, on the one hand, on time-to-solution and, on the other hand, on a comparison-to-experimental variability to select an appropriate level of mesh resolution for the calculations.

Our investigation concludes that the analysis code is adequate to model the low-order bending and torsion dynamics of interest, mainly on the basis of the shell-281 FE of the ANSYS software. Comprehensive mesh refinement studies are performed not only to assess the regime of asymptotic convergence of predictions but also to select a mesh size that yields a numerical uncertainty that is suitable on the basis of the experimental context. The experimental variability observed when performing modal tests of the CX-100 blade with different support setups is quantified and used to guide the selection of mesh resolution. On the basis of the findings discussed in this paper, the FE model is deemed verified and ready for further validation and uncertainty quantification studies discussed in Van Buren *et al.*⁷

ACKNOWLEDGEMENTS

This work is performed under the auspices of the Laboratory Directed Research and Development project 'Intelligent Wind Turbines' at LANL. The authors are grateful to Curt Ammerman, project leader, for his support and acknowledge the technical leadership of Gretchen Ellis for the modeling and analysis of wind turbine blades. The authors also express their gratitude to Krystal Deines, Timothy Marinone and Ryan Schultz, students of the 2010 Los Alamos Dynamics Summer School, for supplying EMA data of the CX-100 wind turbine blade. LANL is operated by the Los Alamos National Security, LLC for the National Nuclear Security Administration of the U.S. Department of Energy under contract DE-AC52-06NA25396.

REFERENCES

1. U.S. Department of Energy. 20% wind energy by 2030: increasing wind energy's contribution to U.S. electricity supply. *Report DOE/GO-102008-2567*, Washington, D.C., 2008.
2. Hahn B, Durstewitz M, Rohrig K. *Reliability of wind turbines*, Wind Energy: Proceedings of the Euromech Colloquium. Springer-Verlag: Berlin, 2007.
3. Walford CA. Wind turbine reliability: understanding and minimizing wind turbine operation and maintenance costs. *Sandia Report, SAND2006-1100*, Sandia National Laboratories, Albuquerque, NM, 2006.
4. Ashwill TD. Blade technology innovations for utility-scale turbines, *AWEA Global Windpower*, Pittsburg, PA, 2006.
5. Ciang CC, Lee JR, Bang HJ. Structural health monitoring for a wind turbine system: a review of damage detection methods. *Measurement Science and Technology* 2008; **19**: 1–20.
6. Paquette JA, Veers PS. Increased strength in wind turbine blades through innovative structural design, *European Wind Energy Conference Proceedings*, Milan, Italy, 2007.
7. Van Buren KL, Mollineaux MG, Hemez FM. Simulating the dynamics of wind turbine blades: part II, model validation and uncertainty quantification, *13th AIAA Non-deterministic Approaches Conference*, Denver, CO, 2010; April 4–7. (Also, Los Alamos report LA-UR-10-5605.)
8. Laird DL. NuMAD user's manual. *Sandia Report, SAND2001-2375*, Sandia National Laboratories, Albuquerque, NM, 2001.
9. Berry D. Design of 9-meter carbon-fiberglass prototype blades: CX-100 and TX-100. *Sandia Report, SAND2007-0201*, Sandia National Laboratories, Albuquerque, NM, 2007.
10. Laird DL, Montoya FC, Malcolm DJ. Finite element modeling of wind turbine blades, *Proceedings of the AIAA/ASME Wind Energy Symposium*, Reno, NV, 2005; 9–17.

11. Hemez FM. Uncertainty quantification and the verification and validation of computational models. In *Damage Prognosis: For Aerospace, Civil and Mechanical Systems*, Inman DJ (ed.). John, Wiley and Sons: West Sussex, England, 2005.
12. Roache PJ. *Verification and Validation in Computational Science and Engineering*. Hermosa Publishers: Albuquerque, NM, 1998.
13. Griffith DT, Carne TG, Paquette JA. Modal testing for validation of blade models. *Wind Engineering* 2008; **32**: 91–102.
14. Veers PS, Laird DL, Carne TG, Sagartz MJ. Estimation of uncertain material parameters using modal test data, *ASME Wind Energy Symposium, 36th AIAA Aerospace Sciences Meeting*, Reno, NV, January 12–15, 1998.
15. Griffith DT, Hunter PS, Kelton DW, Carne TG, Paquette JA. Boundary condition considerations for validation of wind turbine blade structural models, *Society for Experimental Mechanics Annual Conference & Exposition on Experimental and Applied Mechanics*, Albuquerque, NM, June 2009.
16. Griffith DT, Casias M, Smith G, Paquette J, Simmermacher TW. Experimental uncertainty quantification of a class of wind turbine blades, *24th International Modal Analysis Conference*, St. Louis, MO, February 2006. (Also, Sandia report SAND2005-6624C.)
17. Griffith DT, Carne TG. Experimental uncertainty quantification of modal test data, *25th International Modal Analysis Conference*, Orlando, FL, February 2007.
18. Roache PJ. Perspective: a method for uniform reporting of grid refinement studies. *ASME Journal of Fluids Engineering* 1994; **16**: 405–413.
19. Lax PD, Richtmyer RD. Survey of the stability of linear finite difference equations. *Communications in Pure and Applied Mathematics* 1956; **9**: 267–293.
20. Hirt CW. Heuristic stability theory for finite difference equations. *Journal of Computational Physics* 1968; **2**: 339–355.
21. Warming RF, Hyett BJ. The modified equation approach to the stability and accuracy analysis of finite difference methods. *Journal of Computational Physics* 1974; **14**: 159–179.
22. Hemez FM. Functional data analysis of solution convergence. *Los Alamos Report, LA-UR-07-5758*, Los Alamos National Laboratory, Los Alamos, NM, August 2007.
23. Blevins DR. *Formulas for Natural Frequency and Mode Shapes*. Krieger Publishing Company: Malabar, FL, 1993.
24. Deines K, Marinone T, Schultz R, Farinholt K, Park G. Modal analysis and SHM investigation of CX-100 wind turbine blade. *Rotating Machinery, Structural Health Monitoring, Shock and Vibration* 2011; **5**: 413–438.
25. Askeland D, Fulay P, Wright W. *The Science and Engineering of Materials*. CL-Engineering: Stamford, CT, 2010.